A New Non-Heme Iron Environment in *Paracoccus denitrificans* Adenylate Kinase Studied by Electron Paramagnetic Resonance and Electron Spin Echo Envelope Modulation Spectroscopy

Yiannis Deligiannakis,*,‡ Alain Boussac,‡ Hervé Bottin,‡ Véronique Perrier,§ Octavian Bârzu,§ and Anne-Marie Gilles§

Section de Bioénergétique, URA CNRS 2096, Département de Biologie Cellulaire et Moléculaire, CEA Saclay, 91191 Gif-sur-Yvette, France, and Laboratoire de Chimie Structurale des Macromolécules, URA CNRS 1129, Institut Pasteur, 75724 Paris Cedex 15, France

Received January 3, 1997; Revised Manuscript Received May 28, 1997[⊗]

ABSTRACT: Adenylate kinase from the Gram-negative bacterium *Paracoccus denitrificans* (AK_{den}) has structural features highly similar to those of the enzyme from Gram-positive organisms. Atomic absorption spectroscopy of the recombinant protein, which is a dimer, revealed the presence of two metals, zinc and iron, each binding most probably to one monomer. Under oxidizing conditions, the electron paramagnetic resonance (EPR) spectrum of AK_{den} at 4.2 K consists of features at $g = 9.23$, 4.34, 4.21, and 3.68. These features are absent in the ascorbate-reduced protein and are characteristic of a $S = {}^5/_2$ spin system in a rhombic environment with $E/D = 0.24$ and are assigned to a non-heme Fe^{3+} ($S = {}^5/_2$) center. The zero-field splitting parameter D ($D = 1.4 \pm 0.2$ cm^{-1}) was estimated from the temperature dependence of the EPR spectra. These EPR characteristic as well as the difference absorption spectrum (oxidized minus reduced) of AK_{den} are similar to those reported for the non-heme iron protein rubredoxin. Nevertheless, the redox potential of the Fe^{2+}/Fe^{3+} couple in AK_{den} was measured at $+230 \pm 30$ mV, which is more positive than the redox potential of the non-heme iron in rubredoxin. Binding of cyanide converts the iron from the high-spin ($S = {}^5/_2$) to the low-spin ($S = {}^1/_2$) spin state. The EPR spectrum of the non-heme Fe^{3+}($S = {}^1/_2$) in the presence of cyanide has g values of 2.45, 2.18, and 1.92 and spin-Hamiltonian parameters $\boldsymbol{R}/\lambda = 7.4$ and $\boldsymbol{R}/\mu = 0.56$. The conversion of the non-heme iron to the low-spin ($S = {}^1/_2$) state allowed the study of its local environment by electron spin echo envelope modulation spectroscopy (ESEEM). The ESEEM data revealed the existence of ^{14}N or ^{15}N nuclei coupled to the low-spin iron after addition of $KC^{14}N$ or $KC^{15}N$ respectively. This demonstrated that iron in AK_{den} has at least one labile coordination position that can be easily occupied by cyanide. Other possible magnetic interactions with nitrogen(s) from the protein are discussed.

Adenylate kinase (AK,[1] ATP:AMP phosphotransferase, EC 2.7.4.3), a member of the nucleoside monophosphate (NMP) kinase family, is a small monomeric protein involved in energy metabolism (*1*). Recently it was found that the structural motif Cys-X_2-Cys-X_{16}-Cys-X_2-Cys/Asp forms a high-affinity site for zinc binding in AK from *Bacillus stearothermophilus* and *Bacillus subtillis* (*2*, *3*). The zinc atom is coordinated in these proteins by four cysteines or by three cysteines and an aspartic residue, respectively. The existence of such a site with high affinity for metal binding appears to be a common property of the AKs from Gram-positive bacteria, in contrast with the enzymes from Gram-negative species, which are usually devoid of metal ion (*4*).

Adenylate kinase from *Paracoccus denitrificans* (AK_{den}), a Gram-negative bacterium, has structural features highly similar to those of AKs from Gram-positive organisms. Thus, AK_{den} has a metal-binding site with a structural motif Cys-X_2-Cys-X_{16}-Cys-X_2-Cys which is similar to that found in *B. stearothermophilus.* (Perrier et al., manuscript in preparation; see also Figure 6). Interestingly, AK_{den} is a dimer and the recombinant protein binds simultaneously zinc and iron. Iron confers an additional function to AK_{den} that is *in vitro* reduction of the oxidized cytochrome *c*.

To understand the mode of binding and the putative functional role of iron in AK_{den}, the knowledge of its coordination environment is important. Continuous-wave electron paramagnetic resonance (cw EPR) is a powerful tool to study the coordination environment of paramagnetic centers in biological systems (for example, see ref *5* and references therein). Electron spin echo envelope modulation (ESEEM) spectroscopy is a pulsed EPR technique well suited for the study of weak nuclear−electron hyperfine couplings (ref *6* and references therein). ESEEM spectroscopy gives detailed information on the local environments of paramagnetic centers that are not resolvable by cw EPR.

In the present work, we intend to present the basic characterization of the iron binding site in AK_{den} by both continuous-wave EPR and ESEEM spectroscopy. In addition, we report redox titration and experiments that reveal the existence of a labile coordination position, which is easily accessible by small molecules like cyanide.

* Corresponding author: Fax 33 1 69 08 87 17; phone 33 1 69 08 29 40.

‡ CEA Saclay.

§ Institut Pasteur.

⊗ Abstract published in *Advance ACS Abstracts,* July 15, 1997.

[1] Abbreviations: EPR, electron paramagnetic resonance spectroscopy; ESEEM, electron spin echo envelope modulation spectroscopy; AK, adenylate kinase; Tris, tris(hydroxymethyl)aminomethane.

S0006-2960(97)00021-4 CCC: $14.00

MATERIALS AND METHODS

(1) Chemicals. Adenylate kinase gene from *P. denitrificans* was cloned by complementing the thermosensitive *Escherichia coli adk* strain C. R.341T28 (*7*; Perrier et al., manuscript in preparation). The protein was overexpressed and purified by two-step chromatography on blue Sepharose and Ultrogel AcA54 (*7*). Protein iron and Zn contents were determined by atomic absorption spectroscopy. The protein was diluted in pure water (18 MΩ) with 0.1% HNO_3. The calibration of the concentration was done by using standard zinc and iron solutions for atomic absorption purchased from Aldrich. The graphite furnace used was a Perkin-Elmer 2280 spectrometer equipped with an HGA 300 programmer. KCl, KCN, $K_3Fe(CN)_6$, and sodium ascorbate solutions were prepared in Tris-HCl buffer (pH 7.5). The protein in 50 mM Tris, pH 7.5, was concentrated by using a SpeedVac concentrator (Savant) to about 5 mg/mL (≈200 μM). Then the sample was put in a quartz EPR tube and $NaC^{14}N$ or $NaC^{15}N$ was added in the EPR tube. After incubation at 0 °C, ferricyanide (100 μM, final concentration) was added to oxidize the iron from Fe^{2+} into Fe^{3+}.

(2) EPR. Continuous-wave EPR spectra were recorded at liquid helium temperatures with a Bruker ER 200D or ESR300E X-band spectrometer equipped with an Oxford Instruments cryostat. The temperature was monitored with an Oxford ITC-5 temperature controller equipped with a calibrated AuFe (0.007 Cr) thermocouple positioned 5 mm below the lower edge of the sample. As an independent calibration for the temperature at the sample position we have used a 1 mM CuEDTA sample; the Curie behavior was supposed and the point at 4.2 K was considered as reference. Pulsed EPR was done with a Bruker ESP 380 spectrometer previously described (*8*). The ESEEM data result from a three-pulse sequence ($\pi/2$-τ-$\pi/2$-T-$\pi/2$). The amplitude of the stimulated echo as a function of $\tau + T$ was measured at 3580 G. The τ values used was chosen equal to 136 ns to suppress most of the proton-free frequency at around 15 MHz at 3600 G. The minimum interpulse T was 24 ns and was incremented by steps of 8 ns. The $\pi/2$ pulse duration was 16 ns. To remove the unwanted echoes in the three-pulse experiments, the phase cycling procedure described in ref *9* was employed.

(3) Potentiometric Titration. The reduction state of the protein was determined by potentiometric titration followed spectrophotometrically. Potentiometric measurements were performed in an optical cuvette (1 cm optical path), using a platinum plate and a saturated calomel electrode. The cuvette was continuously stirred and flushed with pure argon gas. Adenylate kinase was titrated in 50 mM Tris/HCl, pH 7.5, 1 mM KCl, 1 μM methylene blue, and 1 μM Nile Blue A. The redox potential was adjusted by addition of small volumes of buffered solutions of sodium dithionite, sodium ascorbate, or potassium ferricyanide.

(4) Analysis of the EPR spectra: High-Spin Fe^{3+} ($S = {}^5/_2$). The EPR spectrum of an $S = {}^5/_2$ system can be described by the spin Hamiltonian:

$$H = g_0\beta\,\mathbf{H}\,\mathbf{S} + D[S_z^2 - {}^{35}/_{12} + (E/D)(S_x^2 - S_y^2)] \quad (1)$$

where D and E are the axial and rhombic zero-field splitting parameters, respectively (*10*). The term E/D is a measure of the departure of the electronic environment of the paramagnetic center from axial symmetry; in the proper axis system an axial symmetry corresponds to $E/D = 0$ while a maximally rhombic symmetry corresponds to $E/D = {}^1/_3$ (*11*). For $g_0\beta\,\mathrm{H} \ll |D|$ the magnetic energy levels in the absence of a magnetic field comprise three Kramers doublets. In second-order perturbation theory, the energy level separations are determined from the value of E/D, which in turn can be determined directly from the experimental g values. For $E/D = 0$ the relative energies of the three doublets are 0, $2D$, and $6D$, while for $E/D = {}^1/_3$ they become equidistant, i.e., their relative energies are $0D$, $3.75D$, and $7.5D$, respectively (for a review see ref *5*) and references therein).

(B) Temperature Dependence. Under nonsaturating conditions, changes in the intensity of the EPR signals reflect changes in the Boltzmann population of the energy levels. For a $S = {}^5/_2$ spin system the temperature dependence of the intensity of the EPR signals can be described by

$$I_i(T) = \frac{1}{T}\frac{\exp(-E_i/kT)}{1 + \exp(-E_2/kT) + \exp(-E_3/kT)} \quad (2)$$

where $i = 2$ and 3 for the middle and higher Kramers doublet, respectively. The $1/T$ dependence describes the population difference within each Kramers doublet; the exponential factor takes the Boltzmann distribution of the three doublets into account.

(C) Low-Spin Fe^{3+}($S = {}^1/_2$). In order to simplify the analysis, it is assumed that the t_{2g} and the e_g orbitals are well separated in energy. In the present case this assumption is supported by the Curie behavior of the intensities of the adduct signals versus temperature, indicating that $S > {}^1/_2$ excited states involving the e_g orbitals are not thermally accessible (see Results). When analyzed in the manner suggested by Bohan (*12*), the low-spin EPR spectra are described by the perturbation Hamiltonian

$$H = -\lambda\mathbf{l}\,\mathbf{s} + (\mu/9)\,[3\boldsymbol{l}^2 - \boldsymbol{l}(\boldsymbol{l}+\boldsymbol{1})] + (R/12)(\boldsymbol{l}_+^2 + \boldsymbol{l}_-^2)$$

where λ is the spin-orbit coupling constant and μ and R are the tetragonal and rhombic crystal field splitting constants (ref *12*), and references therein. The eigenfunctions of the Hamiltonian have the form

$$|\psi_i^+\rangle = D\,|\mathrm{d}_{xy}, \alpha\rangle + E\,|\mathrm{d}_{xy}, \beta\rangle + F\,|\mathrm{d}_{xz},\alpha\rangle$$

$$|\psi_i^-\rangle = D\,|\mathrm{d}_{xy}, \beta\rangle + E\,|\mathrm{d}_{xy}, \alpha\rangle + F\,|\mathrm{d}_{xz},\beta\rangle$$

The coefficients D, E, and F can be determined directly from the experimental g values.

(5) Analysis of the ESEEM Data: ^{14}N ($S = {}^1/_2$, $I = 1$). The spin Hamiltonian for an $S = {}^1/_2$, $I = 1$ system is characterized by

$$H = \boldsymbol{g}\,\mu_B\,B_0\,S - g_N\,\mu_N\,B_0\,I + \mathbf{S}\cdot\mathbf{A}\cdot\mathbf{I} + \mathbf{I}\cdot\mathbf{Q}\cdot\mathbf{I}$$

where $\mathbf{A}$ consists of the isotropic contribution A_{iso} and the traceless tensor $\mathbf{T}$ describing the anisotropic hyperfine coupling. The $\mathbf{g}$ tensor has principal values g_x, g_y, and g_z. The nuclear quadrupole interaction, $\mathbf{Q}$, is traceless by definition. In its principal axis system the final term in eq 1 is expressed in the form

$$\mathbf{I}\cdot\mathbf{Q}\cdot\mathbf{I} = K\,[3I_z^2 - I^2 + \eta(I_x^2 - I_y^2)]$$

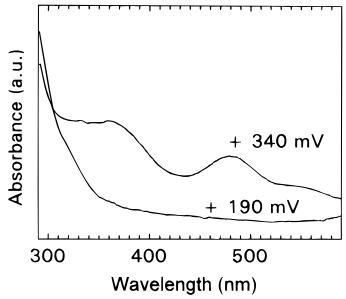

FIGURE 1: Absorption spectra of AK_{den} recorded at +340 and +190 mV (versus NHE).

where K represents the quadrupole coupling constant $e^2qQ/4h$ and η is the asymmetry parameter of the electric field gradient. The energies and eigenfunctions are calculated numerically for each spin manifold and the three-pulse modulations were calculated with the relations derived by Mims (*13*).

RESULTS

(1) Potentiometric Titration of AK_{den}. Figure 1 shows the absorption spectra of the fully reduced and fully oxidized protein at +190 and +340 mV (versus NHE) respectively. The oxidized protein presents an absorption spectrum very similar to that of the oxidized rubredoxin and is characteristic of a non-heme iron in a high-spin state (*14*−*17*).

The midpoint potential of the iron was determined by a potentiometric titration that was followed spectrophotometrically by varying the potential between +190 and +340 mV and by measuring the absorption *maxima* at 370 and 475 nm. The experimental points were fitted by the classical Nernst equation and the apparent midpoint potential found was 230 mV (versus NHE). This value is higher that what is generally reported for iron−sulfur proteins like rubredoxin, i.e., between −60 and +10 mV (refs *18* and *19*, and references therein).

(2) Continuous-Wave EPR Study of the Metal Binding Site. Representative EPR spectra of the AK_{den} recorded at T = 4.2 and 8 K are shown in Figure 2. With no oxidant added, only a fraction of the EPR signal was detected (Figure 2, spectrum A). Addition of 200 μM ferricyanide resulted in significant increase of the intensity of the signals (Figure 2, spectrum B), while addition of sodium ascorbate totally eliminates the signals (not shown). This trend can be explained if we suppose that the signals are due to a paramagnetic center undergoing redox changes due to ferricyanide (oxidation) or ascorbate (reduction) treatment. In all cases, the EPR-detectable spectra show rather well-defined features with no evidence for inhomogeneity. In spectrum B of Figure 2, prominent features are observed at the low-field region at $g \approx 4.3$ and ≈ 9. All the signals are only detectable at cryogenic temperatures (<30 K) and are saturated at high microwave powers. The weak signals in the $g = 2$ region varied from sample to sample and are assigned to nonspecific impurities, mostly copper.

This type of EPR spectrum is characteristic of high-spin iron in rhombic environment, as in non-heme iron metalloproteins and non-heme iron compounds (ref 5 and references therein), and corroborates the atomic absorption analysis, which shows the binding of iron in AK_{den}. Further analysis of the spectra shows that the observed g values are predicted from the spin Hamiltonian (*1*) for $E/D = 0.24$. For $D > 0$

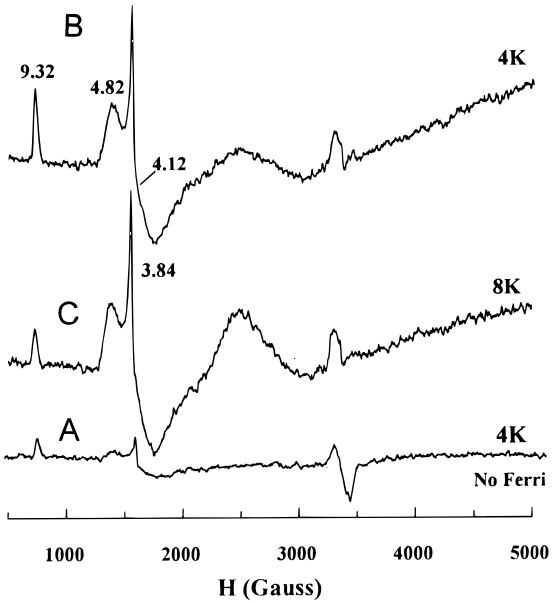

FIGURE 2: X-band EPR spectra of AK_{den} with no addition (A) and after addition of 200 μM ferricyanide at 8 K (C) and at 4 K (B). EPR conditions: modulation amplitude 10 G; modulation frequency 100 KHz; microwave power 8 mW.

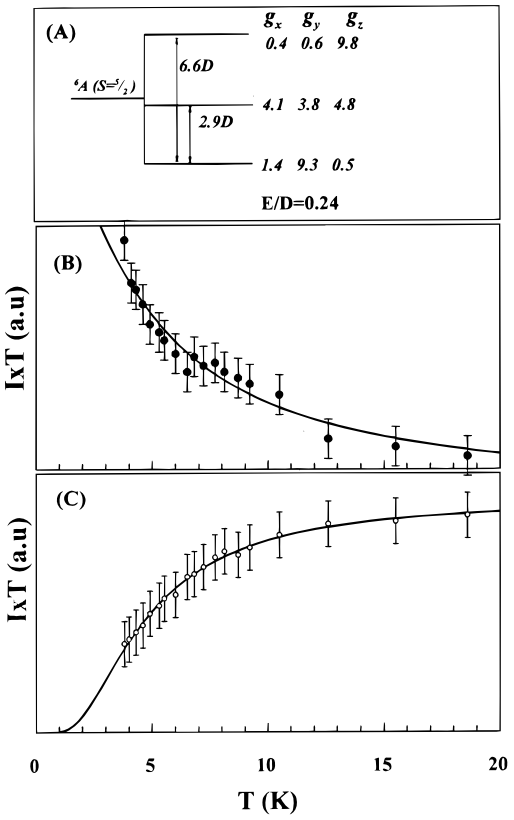

FIGURE 3: (A) Schematic representation of the energy levels of a $S = {}^5/_2$ system for $E/D = 0.24$ and the corresponding effective g-values as they are predicted from the spin Hamiltonian (*1*). (B) Temperature dependence of the EPR signals at $g = 9.32$. (C) Temperature dependence of the EPR signals at $g = 4.84$. The solid lines are the best fit to the data obtained by eq 2 for a single value of $D = 1.4 \pm 0.2$ cm^{-1}

the pertinent energy level diagram is shown in Figure 3A. The predicted effective g-values are given for each Kramer's doublet according to the spin Hamiltonian (*1*). The observed resonances at $g_x = 4.8$, $g_y = 4.1$, and $g_z = 3.8$ arise from transitions in the middle Kramers doublet, while the peak at

Table 1: Effective g-Values and Spin-Hamiltonian Parameters of the Non-Heme Fe^{3+} in AK

high spin ($S = {}^5/_2$)			low spin[a] ($S = {}^1/_2$)		
g-values	E/D	D (cm^{-1})	g-values	R/λ	R/μ
4.85[b]	0.24	1.4 ± 0.2	2.42	7.4	0.56
4.06[b], 3.85[b]			2.18		
9.32[c]			1.92		

[a] According to convention III of Bohan (*12*), we consider the proper g-axis system that in which $\boldsymbol{R} > 0$ and $|\boldsymbol{R}/\mu| \leq {}^2/_3$. [b] Middle Kramers doublet. [c] Lower Kramers doublet.

$g = 9.3$ corresponds to transitions in the ground Kramers doublet. In accordance to this assignment, for $D > 0$, as the temperature is decreased from 20 to 4 K the intensity of the signal at $g = 9.3$ is increased, becoming maximal at 4 K (spectra B and C in Figure 2), while the signals at $g = 4.3$ attain maximum intensity at 6.5 K. For known values of E/D a detailed analysis of the temperature dependence of the EPR signals allows an estimation of the zero-field splitting, and it is presented in the following section.

(A) Determination of the Zero-Field Splitting. The temperature dependence of the intensity of the EPR signals, recorded at nonsaturating microwave power, are shown in Figure 3, panels B ($g = 9.3$) and C ($g = 4.3$). No broadening of the lines is observed in the temperature range from 4 to 20 K. From the analysis according to the spin Hamiltonian (*1*) for $E/D = 0.24$, one obtains $E_3 = 6.6D$ and (for $D > 0$) $E_2 = 2.9D$ as it is shown schematically in Figure 3A. Using these values, the temperature dependence of the signals can be predicted according to eq 2 having the value of D as adjustable parameter; for signals arising from different Kramers doublets of the *same* paramagnetic center, a single value of D should correspond. According to this, the solid lines in Figure 2B are the best fit to the data obtained by eq 2 for a single value of $D = 1.4 \pm 0.2$ cm^{-1}; this value of D means that relative energies of the three Kramers doublets at zero magnetic field are 0, ≈ 4.1 cm^{-1}, and ≈ 9.2 cm^{-1}. The g values and the zero-field splitting parameters are summarized in Table 1.

The EPR characteristics together with the optical absorption spectrum of AK_{den} appear to be similar to what has been reported for mononuclear non-heme iron in biological systems. More specifically, in rubredoxin [$Fe(Cys)_4$] and in protocatechuate dioxygenase the iron centers are spectroscopically similar to the iron center in the present case; however, the iron center in the latter is distinguishable by the degree to which the electronic environment of the iron is alterable by substrates, inhibitors, and other iron ligands.

(B) Effect of Small Molecules. To get more insight into the local environment of the metal site of labile coordination sites we have examined the accessibility of iron by small molecules. After incubation for 30 min at 5 °C in the presence of 1 mM KCN, essentially no low-field signal is detected (Figure 4A). At the same time, new spectral features appear at higher magnetic fields (Figure 4A). Figure 4B shows the kinetics of the decrease of the low-field features of the EPR spectrum (at $g = 9.32$ and 4.8−3.8, ●) and the kinetics of the increase of the high-field features of the EPR spectrum (at $g = 2.45$, 2.18, and 1.92, ○) during incubation at 5 °C in the presence of 1 mM KCN. In a similar sample incubated in the presence of 1 mM KCl instead of KCN, the EPR signals are not changed (data not shown). At early stages (<5 min) the disappearance of the high-spin Fe^{3+} is accompanied by only a small increase of the high-field resonances (Figure 4B). After incubation for 30 min, essentially 100% of the low-field signals became nondetectable; at the same time the high-field peaks attain maximum intensity. Quantification of the signals by the method in (ref *20*) shows that about 80% of the centers that contribute to the low-field EPR signals are converted to the high-field signals after 20 min of incubation of the AK_{den} in the presence of 1 mM KCN.[2]

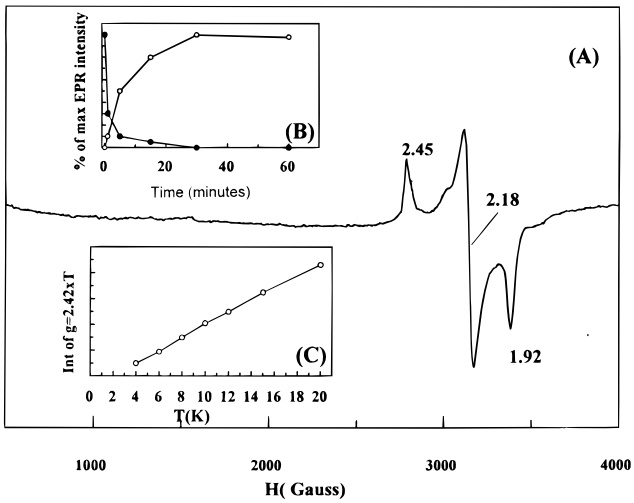

FIGURE 4: (A) EPR spectrum of AK_{den} after incubation for 30 min at 5 °C with 1.6 mM KCN. EPR conditions same as in Figure 2. (B) Kinetics of the decrease of the low-field features of the EPR spectrum (at $g = 9.32$ and $g = 4.8-3.8$, ●) and the kinetics of the increase of the high-field features of the EPR spectrum (at $g = 2.45$, 2.18, and 1.92, ○) during incubation at 5 °C in the presence of 1 mM KCN. (C) Temperature dependence of the intensity of the $g = 2.42$ signal after 30 min od incubation in the presence of 1 mM KCN.

The new EPR signals (at $g = 2.45$, 2.18, and 1.92) are better resolved at lower microwave powers and higher temperatures (15 K) than those recorded in the low-field region. The intensity of the signal when compensated for the $1/T$ (Curie law) dependence is shown in Figure 4C. This behavior is indicative that the signal results from an isolated $S = {}^1/_2$ doublet. The g values of the CN-induced peaks are summarized in Table 1. As it is discussed below, these characteristics are reminiscent of low-spin Fe^{3+} systems and are assigned to the low-spin form of the iron of AK; the transition to the low-spin state is induced by the treatment with CN. This molecule is a ligand with high affinity for iron that converts the iron to low-spin state upon binding it (*16*, *21*, *22*).

To test a possible effect of salt (i.e., of the ionic strength) on the protein, AK_{den} was incubated with concentrations of KCl up to 40 mM. This did not alter the AK_{den} EPR spectrum. This contrasts with the effect of KCN, where much lower concentrations (<2 mM) and incubation times (<1 min) changed the AK_{den} EPR spectrum. Taken altogether, these experiments demonstrate that the effect of KCN is specific.

[2] After 60 min of incubation of the AK_{den} in the presence of 5 mM KCN, in addition to the spectrum shown in Figure 2 the EPR spectrum contains a second set of high-field peaks with similar intensities. The second set of g values are identical to those obtained from $FeCl_2$ solution with 5 mM KCN and are assigned to nonspecific iron coordinated by CN.

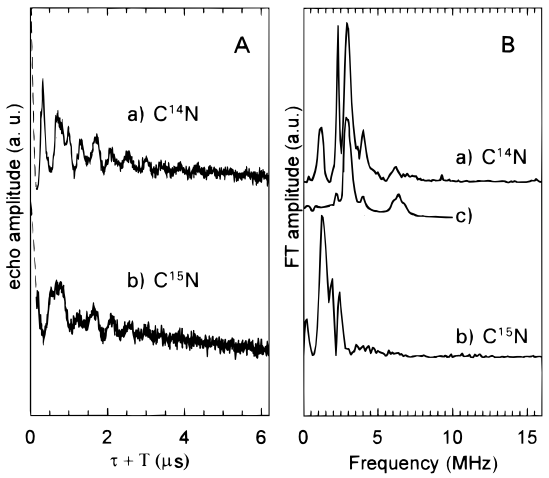

FIGURE 5: (A) ESEEM in the time domain of the $C^{14}N$-treated sample (spectrum a) and $C^{15}N$-treated sample (spectrum b). (B) Frequency domain of the ESEEM shown in panel A. Spectrum c in panel B shows a calculated curve using the parameters described in Table 2. The amplitude of the echo resulted from the sequence ($\pi/2$-τ-π/2-T-$\pi/2$) with $\pi/2 = 8$ ns, $\tau = 136$ ns, and $T_{min} = 24$ ns. Other instrument settings: temperature, 4.2 K; microwave frequency, 9.6 GHz; shot repetition time, 16 ms.

(3) Electron Spin Echo Envelope Modulation Spectroscopy. Electron spin echo envelope modulation spectroscopy is a powerful method to detect any atom that possesses a nuclear spin [e.g., H ($I = {}^1/_2$), ^{14}N ($I = 1$), ^{15}N($I = {}^1/_2$), P ($I = {}^1/_2$) etc.] in the environment of the electronic spin (see, for example, ref *23*). Due to the fast relaxation of Fe^{3+} in the high-spin state ($S = {}^5/_2$), the detection of an electron spin echo requires temperatures below 4 K (see, for example, ref *24*). At 4 K the iron should be converted into the low-spin state ($S = {}^1/_2$), which relaxes more slowly, to be detected. As we have shown, this conversion can be done by the addition of cyanide.

The ESEEM measurements were done at 3580 G ($g = 1.92$), i.e., on the low-field peak. As indicated above, the low-spin Fe^{2+} was oxidized with ferricyanide. As it was used in stoichiometric amount with the protein and since it was fully converted into the non-EPR-active ferrocyanide after the oxidation of the protein, no modulation from this species was expected to contaminate the ESEEM data. Figure 5A shows the ESEEM in the time domain of the $C^{14}N$-treated sample (spectrum a). To discriminate frequencies arising from the nitrogen of cyanide to those of the protein, the measurements were also done with $C^{15}N$-treated sample (Figure 5A, spectrum b). Figure 5B shows the frequency domain of the ESEEM shown in Figure 5A. The main peaks in spectrum a are 1.22, 2.32, 2.93, 4.03, and 6.23 MHz, and in spectrum b, 1.22, 1.96, and 2.44 MHz.

The observed changes demonstrate that at least a part of the observed modulation originates from coupling of the low-spin iron with one or more nitrogens of CN. This is direct evidence that CN binds in the close vicinity of the iron in AK_{den}.

DISCUSSION

The EPR characteristics, the zero-field splitting $D = +1.4$ cm^{-1}, and the rhombicity parameter $E/D = 0.24$ found in the present case are similar to those observed for the non-heme Fe^{3+}($S = {}^5/_2$) in the rubredoxin ($D = +1.92$ cm^{-1}, $E/D = 0.28$) isolated from *Clostridium pasteurianum* (see refs *25* and *26* for a review). We consider that the stereochemical constrains imposed by the protein environment determine the ligand field parameters *E* and *D*. In the rubredoxin, the structural motif Cys-X_2-Cys-X_{16}-Cys-X_2-Cys forms the binding pocket of the non-heme ferric center. In AK_{den} the structural motif Cys-X_2-Cys-X_{16}-Cys-X_2-Cys that has been postulated to form the iron binding site bears striking similarities with that in the rubredoxin and are is line with the similar ligand field parameters in the two cases. Furthermore these similarities are in line with the similar optical absorption spectra in the two cases.

According to the present EPR study, the iron site of native AK_{den}, which is a dimer, is apparently homogeneous. In the case of binding of two iron atoms in AK_{den} (one per monomer) then the ligand field parameters, i.e., the coordination environments, of the iron atoms are identical and the iron−iron distance should be large since no magnetic interaction is evident. In fact, there are examples of other dimeric non-heme iron proteins that bind one iron atom per monomer. For example in the transferrins and in the desulfodoxin from *Desulfovibrio gigas* the two iron atoms give similar EPR spectra. No magnetic interaction between two metal sites has been detected by EPR and this has been interpreted as being due to the large distance (calculated as equal to 41.6 ± 2.8 Å) between the two metal-binding sites (*27*). This has been confirmed by the 3D structure of transferrin, from which the iron−iron distance has been measured equal to 42 Å (*28*).

On the basis of the homology between the amino acid sequence of AK_{den}, deduced from the nucleotide sequence of the gene, and the AK from *B. stearothermophilus* and *B. subtilis* (*2*, *3*) (see also Figure 6), we expect for the metal binding site to be located into the INSERT domain of the protein and to be exposed to the solvent. This is in qualitative agreement with the facile accessibility of the iron in AK_{den} by exogenous molecules like CN.

An important finding of this work is that the metal site has a labile coordination position which can be occupied by extrinsic molecules like CN. The conversion of a number of non-heme iron centers from the high- to the low-spin state due to CN binding has been reported in a number of non-heme iron proteins, for example protocatechuate dioxygenase (*21*), transferrins (*16*), the reaction center of photosystem II (*22*), and a 4-Fe ferredoxin in *Pyrococcus furiosus* (*29*). The conversion of the non-heme Fe^{3+}($S = {}^5/_2$) to the low-spin ($S = {}^1/_2$) after CN binding is in clear contrast with the case of other spectroscopically similar non-heme iron centers in rubredoxins. On the other hand, the high-spin and low-spin EPR spectra are quite similar to those reported for protocatechuate dioxygenase (*21*). In all these cases the binding of more than one molecule of CN is required for the formation of the low-spin state. In photosystem II and in transferrins the CN binds on the iron after the displacement of a bicarbonate molecule, while in the protocatechuate dioxygenase the CN has to displace a H_2O molecule. In the latter case a single CN molecule, when bound on the iron, induces a modification of the ligand field while the iron remains in the high-spin state. In the latter case a major rearrangement was suggested to take place that would allow the binding of a second CN molecule with a subsequent conversion to low spin (*21*).

In this context we consider that the conversion of the iron from the high-spin ($S = {}^5/_2$) to the low-spin ($S = {}^1/_2$) state

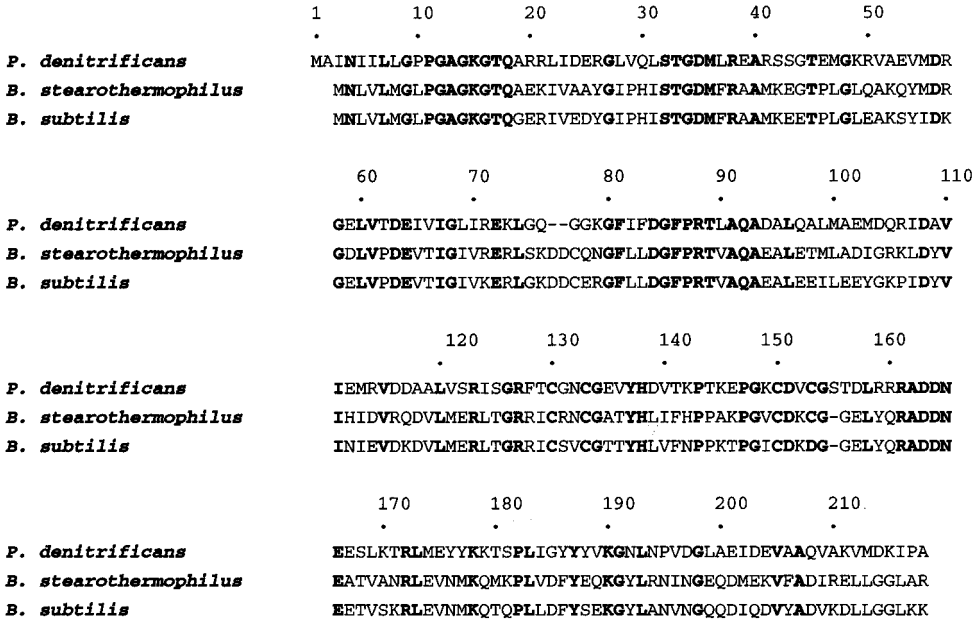

FIGURE 6: Alignment of amino acid sequences of adenylate kinase from *Paracoccus denitrificans*, *Bacillus stearothermophilus*, and *Bacillus subtilis* as deduced from the nucleotide sequences of the corresponding genes. The conserved residues are shown in boldface type.

Table 2: Hyperfine and Quadrupole Coupling Parameters of $C^{14}N$ Bound to the Non-Heme Iron of AK_{den}[a]

hyperfine coupling	quadrupole coupling
$A_{xx} = 1.85$ MHz (error 0.05)	$Q = 3.82$ MHz
$A_{yy} = 1.55$ MHz	$\eta = 0.03$ (error 0.01)
$A_{zz} = 1.35$ MHz	
$a = 0, \beta = 20, \gamma = 0$	$u = 0, v = 20, w = 0$

[a] The values above correspond to the best fit of the peaks at 2.9/4.0/6.3 MHz in spectrum c, Figure 5B. The two sets of angles are the Euler angles of tensors **A** (a, β, γ) and **Q** (u, v, w) relative to the **g** tensor.

is induced by the binding of one or more CN molecules on the non-heme iron. Binding of CN to the non-heme iron is further demonstrated by simulation of spectrum a in Figure 5B. This simulation of the couplings between Fe^{3+} ($S = {}^1/_2$) and the ^{14}N of CN included anisotropic **g** tensor and orientation selection (spectrum c, Figure 5B). The best fit to the peaks at 2.9/4.0/6.3 MHz was achieved by using quadrupole couplings of CN. The results are described in Table 2. The Q and η values almost coincide with the Q and η values reported for $C^{14}N$ in $K_3Fe^{III}(CN)_6$ (*30*), confirming the suggested binding of CN on the iron via the carbon.

We may consider two possible mechanisms associated with the binding of cyanide: (a) the CN binding site(s) is(are) originally nonoccupied by ligand(s) or (b) the CN coordination position(s) is(are) occupied by another molecule. In case b, the binding of CN would require the displacement of at least one ligand. If this is the case for the iron in AK_{den} then the ligand under consideration is unknown. It is noticed that in all three aforementioned cases of CN binding in non-heme iron proteins it appears that mechanism b is encountered. In all cases CN replaces non-protein ligands (bicarbonate or H_2O).

The disappearance of the high-spin iron EPR signals after treatment with 1 mM KCN (250-fold excess) at short incubation times (<1 min) without being accompanied by the appearance of the low-spin adduct is not easily understandable. The low-spin signals appear significantly only after prolonged incubation, typically 5 min. We may consider the possibility that treatment with CN modifies the properties of the high-spin iron in such a way that it initially becomes an EPR-silent state. A change in the redox potential to a more positive value with a subsequent reduction of the iron to the Fe^{2+} ($S = 2$) state would be consistent with the disappearance of the Fe^{3+} ($S = {}^5/_2$) EPR signals. If this assumption is correct, then the new E_m has to be higher than the E_m in the present case (i.e., higher than +230 mV). More extended studies like enzymatic significance of CN binding and details on the binding mechanism will be the subject of future works.

Iron is frequently encountered in proteins and may play either a functional role, a structural role, or both. The value of the redox potential is an essential parameter for the characterization of a metalloprotein and, in certain cases, for the determination of its physiological function. Rubredoxins constitute a group of non-heme iron proteins with a rather narrow range of redox potentials between −60 and + 10 mV(see ref *19* and references therein). The redox potential of the iron E_m, +230 mV in AK_{den}, is higher than the E_m for a rubredoxin-type iron center; thus at ambient redox potential the iron is predominantly in the ferrous Fe^{2+} ($S = 2$) state. Although the correlation of redox potential with the type of metal environment is not always straightforward, the existence of a non-sulfur ligand may explain the elevated redox potential; the existence of non-sulfur ligands, i.e., N or O, parallels the more positive redox potentials in other non-heme iron centers. Histidine is a common ligand of non-heme iron in proteins, i.e., one His in transferrins, three His in soybean lipoxygenase (*31*), and four His in photosynthetic reaction centers (*32*) and protocatechuate dioxygenase, for examples.

The ESEEM data indicate the existence of nitrogen nuclei that originate from cyanide but also probably from the protein. Indeed, in Figure 5B peaks around 2.3 and 1.2 MHz in spectrum a (in the presence of $C^{14}N$) are still present in the presence of $C^{15}N$. From the protein sequence (Figure 6), H138 could be a candidate (*3*). Although this amino acid has been shown to not participate in Zn^{2+} binding in AK

from *B. subtilis*, nothing argues against the possibility that His138 participates in the iron binding in AK from *P. denitrificans*. Moreover, the observed couplings probably do not arise from nitrogen(s) directly coordinated to the iron. This kind of directly coordinated nitrogen(s) has been detected in model compounds (*33*, *34*) and in proteins (*34*−*37*). This is typically characterized by an A_{iso} at around 4−5 MHz. Such a coupling is expected to result in an ESEEM spectrum consisting of just two prominent features corresponding to the double quantum $\delta m_I = 2$ transitions in the two spin manifolds (*38*). This has been experimentally observed in ESEEM spectra recorded on iron centers where one typically observes one peak at 2−4 MHz and a second one at 5−7 MHz (refs *34* and *36* and references therein). In $AK_{den,}$ the low-frequency domain does not contain such features (see Figure 5). We cannot assign the observed peaks to a certain type of nitrogen coupling due to the lack of knowledge of the quadrupole coupling constants. Nevertheless, our simulations of the ESEEM data in the time and frequency domain clearly indicate that the low-frequency features, apart from those that originate from CN, arise from weakly hyperfine couplings in the frequency range of 1 MHz or less. This weak coupling does not necessarily imply the presence of a direct nitrogen coordination to the metal ion. For example, in various Fe−S proteins analogous weak couplings have been detected by ESEEM and electron nuclear double resonance spectroscopy (ENDOR) and assigned to noncoordinated nitrogens (refs *35*, *36*, *39*, and *40* and references therein). Specific mutation of His138 in AK_{den} would certainly solve this question.

REFERENCES

1. Noda, L. H. (1973) in *The Enzymes (3rd Ed.)* (Boyer, P. D., Ed.) pp 279−305, Academic Press, New York.
2. Glaser, P., Presecan, E., Delepiere, M., Surewicz, W. K., Mantsch, H. H., Bârzu, O., and Gilles, A.-M. (1992) *Biochemistry 31*, 3038−3043.
3. Perrier, V., Surewicz, W. K., Glaser, P., Martineau, L., Craescu, C. T., Fabian, H., Mantsch, H. H., Bârzu, O., and Gilles, A.-M. (1994) *Biochemistry 33*, 9960−9967.
4. Gilles, A.-M., Glaser, P., Perrier, V., Meier, A., Longin, R., Sebald, M., Maignan, L., Pistotnik, E., and Bârzu, O. (1994) *J. Bacteriol. 176*, 520.
5. Gaffney, B., and Silverstone, H. J. (1993) in *Biological Magnetic Resonance* (Berliner, L. J., and Reuben, J., Eds.) Vol. 13, pp 1−55, Plenum Press, New York.
6. Dikanov, S. A., and Tsvetkov, Y. D. (1992) *ESEEM Spectroscopy*, CRC Press, Boca Raton, FL.
7. Saint Girons, I., Gilles, A.-M., Margarita, D., Michelson, S., Monnot, M., Fermandjian, S., Danchin, A., and Bârzu, O. (1987) *J. Biol. Chem. 262*, 662.
8. Deligiannakis, Y., Boussac, A., and Rutherford, A. W. (1995) *Biochemistry 34*, 16030.
9. Kevan, L. (1990) in *Modern Pulsed and Continuous Wave Electron Spin Resonance* (Kevan, L., and Bowman, M. K., Eds.) pp 231−266, Wiley Interscience, New York.
10. Pilbrow, J. R. (1991) *Transition Ion Electron Paramagnetic Resonance*, Oxford Science Publications. Clarendon Press, Oxford, England.
11. Blumberg, W. E. (1967) in *Magnetic Resonance in Biological Systems* (Ehrenberg, A., Mälmstrom, B. C., and Vänngard, T., Eds.) pp 119−129, Pergamon, Oxford, England.
12. Bohan, T. L. (1977) *J. Magn. Reson. 26*, 109.
13. Mims, W. B. (1972) *Phys. Rev. B5*, 2409 and 3542.
14. Eaton, G. A., and Lovenberg, W. (1973) in *Iron-Sulfur Proteins* (Lovenberg, W., Ed.) pp 131−162, Academic Press, New York and London.
15. Cavagnero, S., Zhou, Z. H., Adams, W. W., and Chan, S. (1995) *Biochemistry 34*, 9865.
16. Swope, S. K., Chasteen, N. D., Weber, K. E., and Harris, D., C. (1988) *J. Am. Chem. Soc. 110*, 3835.
17. Holm, R. H., Kennepohl, P., and Solomon, E. I. (1996) *Chem Rev. 96*, 2239.
18. Cammack, R. (1992) *Adv. Inorg. Chem. 38*, 281.
19. Swartz, P. D., and Ichiye, T., (1996) *Biochemistry 35*, 13772.
20. Aasa, R., and Vänngard, T. (1975) *J. Magn. Reson. 19*, 308.
21. Whittaker, J. W., and Lipscomb, J. D. (1984) *J. Biol. Chem. 259*, 4487.
22. Sanakis, Y., Petrouleas, V., and Diner, B. A. (1994) *Biochemistry 33*, 9922.
23. Schweiger, A. (1991) *Angew. Chem., Int. Ed. Engl. 30*, 265.
24. Dubach, J., Gaffney, B. J., More, K., Eaton, G. R., and Eaton, S. S. (1991) *Biophys. J. 59*, 1091.
25. Peisach, J., Blumberg, W. E., Lode, E. T., and Coon, M. J. (1971) *J. Biol. Chem. 246*, 5877.
26. Hagen, W. R. (1992) *Adv. Inorg. Chem 38*, 165.
27. Zweier, J. L. (1983) *J. Biol. Chem. 258*, 13759.
28. Baker, E. N., Rumball, S. V., and Anderson, B. F. (1987) *Trends Biochem. Sci. 12*, 350.
29. Telser, J., Smith, E., Adams, M. W. W., Conover, R., C., Johnson, M. K., and Hoffman, B. H. (1995) *J. Am. Chem. Soc. 117*, 5133.
30. Willens, J. P., Reijerse, E. J., and De Boer, E. (1994) *Mol. Phys. 83*, 1155.
31. Scarrow, R. C., Trimitsis, M. G., Buck, C. P., Grove, G. N., Cowling, R. A., and Nelson, M. (1994) *Biochemistry 33*, 15023.
32. Michel, H., and Deisenhofer, J. (1988) *Biochemistry 27*, 1.
33. Mims, W. B., and Peisach, J. (1978) *J. Chem. Phys. 69*, 4921.
34. Peisach, J., Mims, W. B., and Davis, J. L. (1979) *J. Biol. Chem. 254*, 12379.
35. Houseman, A. L. P., Oh, B.-H., Kennedy, M. C., Fan, C., Werst, M. M., Beinert, H., Markley, J. L., and Hoffman, B. M. (1992) *Biochemistry 31*, 2073.
36. Dikanov, S. A., Xun, L., Karpiel, A. B., Tyryshkin, A. M., and Bowman, M. K. (1996*) J. Am. Chem. Soc. 118*, 8409.
37. McKracken, J., Pemper, S., Benkovic, S. J., Villafranca, J. J., Miller, R. J., and Peisach, J. (1988) *J. Am. Chem. Soc. 110*, 1069.
38. Flanagan, H. L., and Singel, D. J. (1987) *J. Chem. Phys. 89*, 5606.
39. Shergill, J. K., Ioannou, C. L., Mason, J. R., and Cammack, R. (1995) *Biochemistry 34*, 16533.
40. Dikanov, S. A., Tyryshkin, A. M., Felli, I., Reijerse, E. J., and Huttermann, J. J. (1995) *J. Magn. Reson. Ser. B 108*, 99.

BI970021E